RSC Advances

PAPER

View Article Online
View Journal | View Issue

Cite this: *RSC Adv.*, 2014, **4**, 45300

Coulomb explosion and dissociative ionization of 1,2-dibromoethane under an intense femtosecond laser field

Hua Wu,[a] Shian Zhang,*[a] Yan Yang,[ab] Shengzhi Sun,[a] Jian Zhang,[a] Li Deng,[a] Tianqing Jia,[a] Zugeng Wang[a] and Zhenrong Sun[a]

Received 2nd July 2014
Accepted 10th September 2014

DOI: 10.1039/c4ra06121g

www.rsc.org/advances

Coulomb explosion and dissociative ionization of 1,2-dibromoethane are experimentally investigated in a near-infrared (800 nm) femtosecond laser field by dc-slice imaging technology. The sliced images of the fragment ions $C_2H_4Br^+$, Br^+, $C_2H_4^+$, Br_2^+ and CH_2Br^+ are obtained, and their corresponding kinetic energy releases (KERs) and angular distributions are calculated. It is confirmed that the high-KER components come from Coulomb explosion of 1,2-$C_2H_4Br_2^{2+}$, while the low-KER components come from dissociative ionization of 1,2-$C_2H_4Br_2^+$. Furthermore, the dissociation pathway leading to $C_2H_4^+$ and Br_2 is theoretically simulated, and the results show that the singly charged precursor overcomes an energy barrier to dissociate *via* an asynchronous concerted mechanism after undergoing isomerization.

I. Introduction

The atomic or molecular response to an intense femtosecond laser field is a subject of growing interest and has exhibited a rich variety of phenomena, such as multi-photon ionization (MPI),[1,2] charge resonant enhanced ionization (CREI),[3] dissociative ionization (DI),[4] and Coulomb explosion (CE).[5,6] These corresponding phenomena can be utilized to study atomic or molecular dynamical processes, and therefore have attracted considerable attention of researchers in the past decades. In the atmosphere, hydrocarbon bromide can greatly damage the stratosphere ozone layer,[7–9] and therefore their photoionization and photodissociation dynamics in intense laser field have been an active field of research. By now, many researchers have focused their energies on the simple and small alkyl bromides, such as CH_3Br,[10–12] CH_2Br_2,[13] CF_2Br_2,[14] and $CHBr_3$.[15,16] However, studies on photoionization and photodissociation of the long-chained multibrominated alkyls are relatively lack because of their complicated structure of electronic states arising from the multi C–Br bonds and the long chain.

When the long-chained dibromide alkyls are irradiated by the laser field, the resulting dissociation process can be quite complicated, and a number of dissociation channels from different mechanisms are likely to be accessed. In addition to the selection of breaking a single C–Br bond,[17] three-body formation or bromine molecular elimination by either a stepwise or a concerted (synchronous or asynchronous) mechanism may take place in the dissociation process of these molecules.[18–20] In the photodissociation studies of 1,1 and 1,2-$C_2H_4Br_2$ with the ultraviolet (248 nm) laser by product translational spectroscopy,[18] Lin and co-workers observed that 1,1-$C_2H_4Br_2$ would undergo a prompt C–Br bond fission, which was the same as the case of CH_2Br_2, and a second Br atom could be released by additional photon absorption. However, 1,2-$C_2H_4Br_2$ fragmented into the triple products Br (fast) + Br (slow) + C_2H_4 by an asynchronous concerted mechanism. Furthermore, they also studied the dissociation of CH_2XCH_2Y (X, Y = Br, Cl) with the deep ultraviolet (193 nm) laser,[19] and found that all the title molecules dissociated into three fragments X + Y + C_2H_4 *via* an asynchronous concerted process, but the Br_2 fragments were not observed in these experiments. When a cavity ring-down absorption spectroscopy technique was employed,[20] Chang and co-workers observed the bromine molecular elimination channel of 1,1 and 1,2-$C_2H_4Br_2$, and Br_2 was found to eliminate asynchronously from the highly vibrational levels of the ground state surface by *ab initio* calculation.

The previous photodissociation studies of 1,2-$C_2H_4Br_2$ were performed under ultraviolet excitation in weak laser field, while the studies under near-infrared excitation in intense laser field have not been reported to our knowledge. In this paper, we present an investigation of the CE and DI of 1,2-$C_2H_4Br_2$ under the near-infrared femtosecond laser field with the laser wavelength of 800 nm and the pulse duration of 80 fs. The dc-slice velocity imaging technology, which can provide information about the velocity and angular distributions of the target ions at the same time,[21,22] is employed to study the photodissociation process of 1,2-$C_2H_4Br_2$. The sliced images of these fragment ions at different laser intensities are measured, and their

[a]State Key Laboratory of Precision Spectroscopy, Department of Physics, East China Normal University, Shanghai 200062, P. R. China. E-mail: sazhang@phy.ecnu.edu.cn; zrsun@phy.ecnu.edu.cn

[b]State Key Laboratory of High Field Laser Physics, Shanghai Institute of Optics and Fine Mechanics, Chinese Academy of Sciences, Shanghai 201800, P. R. China

corresponding KERs and angular distributions are extracted and calculated. It is found that both the CE of 1,2-$C_2H_4Br_2^{2+}$ and the multi-photon DI of 1,2-$C_2H_4Br_2^+$ coexist in our experiment, and the CE and DI channels are assigned by observing the KERs and angular distributions of these fragment ions. Furthermore, the DI pathway leading to $C_2H_4^+$ and Br_2 is calculated by GAUSSIAN 09 software packages with B3LYP functional, and our results show that the singly charged isomer dissociates into $C_2H_4^+$ and Br_2 *via* an asynchronous concerted mechanism.

II. Experimental setup

Our home-built experimental setup of dc slice ion-imaging system has been described in our previous paper,[23–25] and therefore only a brief description is given here. Our experimental setup consists of a home-built time-of-flight (TOF) mass spectrometer and a two-dimensional (2D) position sensitive detector. The TOF mass spectrometer is divided into the source chamber and the main chamber by a skimmer, and both the source chamber and the main chamber are pumped to low background pressures of 2.2×10^{-7} and 4.0×10^{-8} mbar, respectively.

Liquid sample of 1,2-$C_2H_4Br_2$ molecules (Sinopharm Chemical Reagent Co., Ltd., 99.7+ % purity) are carried by helium gas at 1 atm and introduced into the reaction region (*e.g.* the main chamber) by a pulsed valve. The linearly polarized femtosecond laser pulses from the Ti-sapphire amplifier with the central wavelength of 800 nm, the pulse duration of 50 fs, and the repetition rate of 1 KHz are used as excitation source. The output femtosecond laser pulses are focused into the reaction region by a lens with 40 cm focal-length, and intersect with the leading edge of the pulsed super-sonic molecular beam to minimize the cluster formation. The interaction position of the molecular beam and the laser pulses is in the middle of the repeller and extractor plates of a multi-stage ion lens. The generated fragment ions are extracted and accelerated by ion lens and projected onto the 2D detector composed of Micro-channel Plate (MCP)/Phosphor Screen (PS) detector. The electrons emitted from the MCP are accelerated toward a PS, and the phosphorescence is recorded by a photomultiplier tube (PMT) to obtain TOF mass spectra and imaged with a charge coupled device camera (CCD) to acquire sliced images. A rotatable crystal quartz half-wave plate and a Glan laser calcite polarizer are used as a variable attenuator for the laser beam. The laser intensity at the focus area is calibrated by the Ar^{2+}/Ar^+ ratio proposed by Guo *et al.*,[26] and the calibrated intensities are 5.0×10^{13}–1.6×10^{14} W cm^{-2}. All the timing sequence control in this experiment is performed by a digital delay pulse generator (Stanford Research DG535).

III. Results and discussion

Fig. 1 shows the TOF mass spectrum of 1,2-$C_2H_4Br_2$ with the laser intensity of 1.3×10^{14} W cm^{-2}. Because of the Br isotopes (79 amu and 81 amu), the bromine-containing fragment ions exhibit multiple peak structures. Considering the laser pulse duration of 80 fs in our experiment, the ionization followed by dissociation process is the responsible mechanism, but no singly or doubly charged parent ions is observed, which indicates that the chemical bond fissions of 1,2-$C_2H_4Br_2$ are easy to occur in the intense femtosecond laser field. The fragment ions $C_2H_4Br^+$ and Br^+ resulting from C–Br bond fission are observed at the laser intensity of 5.6×10^{13} W cm^{-2}, while the fragment ion CH_2Br^+ resulting from C–C bond fission is observed at the laser intensity of 6.5×10^{13} W cm^{-2}, which implies that the C–Br bond fission is easier to occur than the C–C bond fission in our experiment. The fragment ion Br_2^+ resulting from two C–Br bond fissions is observed at the laser intensity of 1.1×10^{14} W cm^{-2}, and its formation mechanism has been detailed studied in our previous work.[25] The multi-charged fragment ions Br^{2+}, C^{2+}, and C^{3+} are respectively observed at the laser intensity of 6.5×10^{13}, 1.1×10^{14}, and 1.6×10^{14} W cm^{-2}, which is correlated with their appearance energy that is increase from Br^{2+}, C^{2+} to C^{3+}. Additionally, the fragment ions CH_n^+ (n = 0–2) and $C_2H_m^+$ (m = 0–3) are also observed, and their yields will increase more rapidly than other fragment ions with the increase of the laser intensity, which may be due to the secondary dissociation. In the following discussion, we mainly focus on the photodissociation process of these fragment ions $C_2H_4Br^+$, Br^+, $C_2H_4^+$, Br_2^+ and CH_2Br^+ *via* the C–Br and C–C bond fissions.

The photodissociation process of polyatomic molecules is quite complex, and the fragment ions with the same m/q may come from different dissociation channels. The dc-sliced imaging technique can provide a well-established method to discriminate these different dissociation channels. Fig. 2 shows the sliced images of these fragment ions $C_2H_4Br^+$, Br^+, $C_2H_4^+$, Br_2^+ and CH_2Br^+, together with the velocity distributions calculated from their corresponding sliced images with the laser intensity of 1.3×10^{14} W cm^{-2}. Here, all velocity distributions are fitted with multiple Gaussian functions, and also the peak velocities and their corresponding KER values are given. To understand the photodissociation process of 1,2-

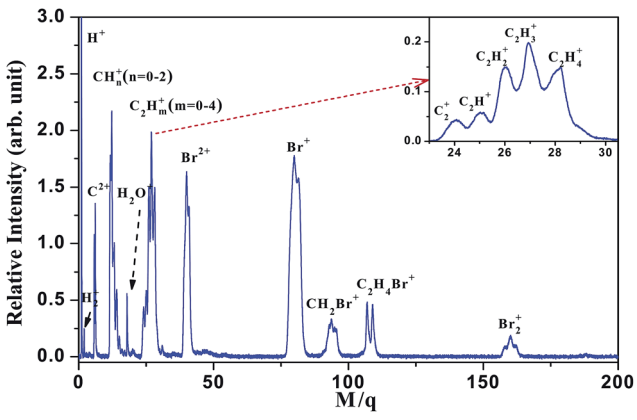

Fig. 1 TOF mass spectrum of 1,2-$C_2H_4Br_2$ irradiated by the near-infrared (800 nm) femtosecond laser pulses with the laser intensity of 1.3×10^{14} W cm^{-2}. The insert is the enlarged mass spectrum of the fragment ions $C_2H_m^+$ (m = 0–4).

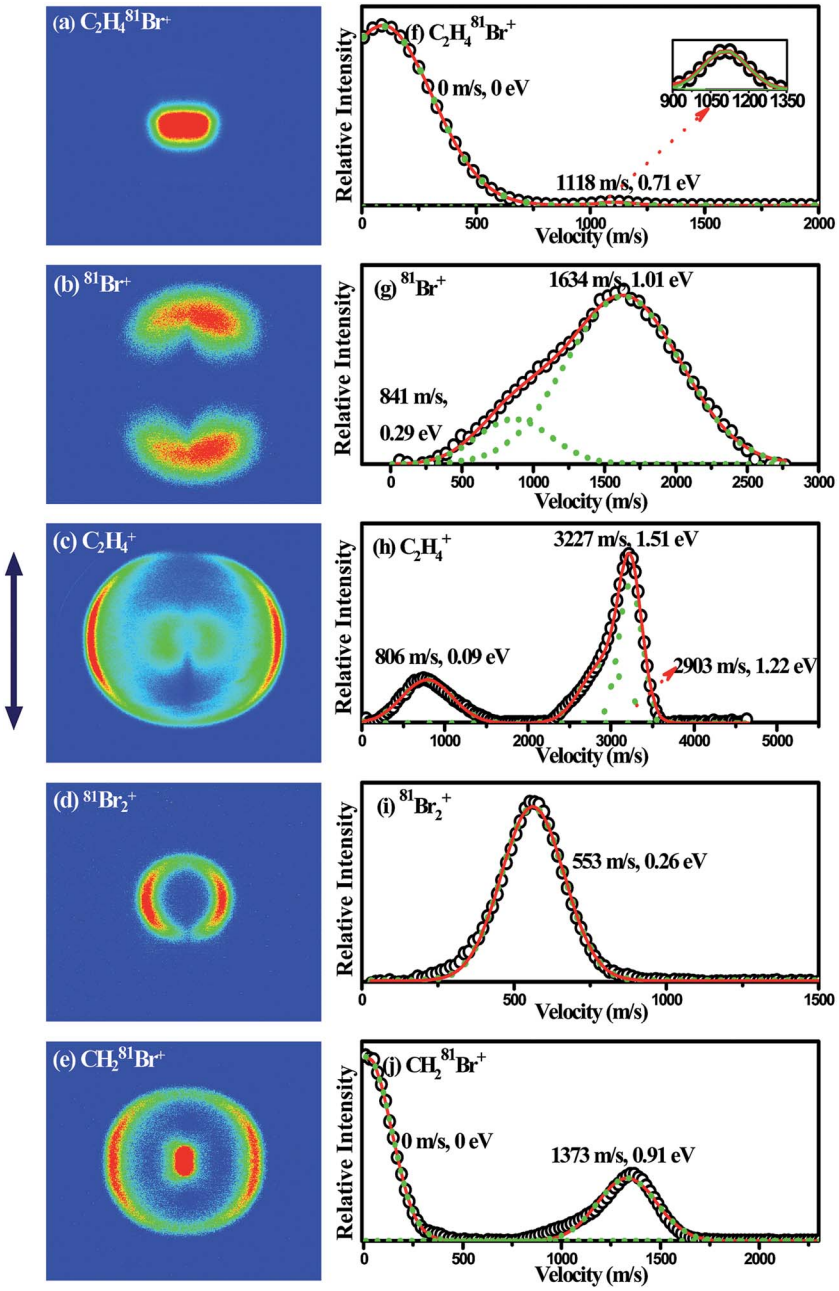

Fig. 2 DC sliced images of these fragment ions $C_2H_4Br^+$ (a), Br^+ (b), $C_2H_4^+$ (c), Br_2^+ (d) and CH_2Br^+ (e) and their corresponding velocity distributions ((f)–(j)) with the laser intensity of 1.3×10^{14} W cm^{-2}. The black circles (○) are the experimental data and the red solid lines (——) are the simulated results by multiple Gaussian functions. The dark blue double-headed arrow represents the laser polarization direction.

$C_2H_4Br_2$, it is critical to assign the photodissociation channels of these fragment ions. Usually, the fragment ions with high KER should result from the CE process while those with low KER should result from the multi-photon DI process.[23,27,28] Next we assign the photodissociation channels of these fragment ions $C_2H_4Br^+$, Br^+, $C_2H_4^+$, Br_2^+ and CH_2Br^+ on the basis of the two processes.

When the gaseous molecules are exposed to the intense femtosecond laser field, which can be multiply ionized to the highly charged parent ions and then promptly dissociate into fragment ions by the Coulomb repulsive force. In the two-body CE model, the two fragment ions separated by the Coulomb repulsive force should satisfy the law of momentum conservation. That is to say, the KERs of the two fragment ions exist the following relationship[27,29]

$$\frac{\mathrm{KER}(\mathrm{X}^{p+})}{\mathrm{KER}(\mathrm{Y}^{q+})} = \frac{M(\mathrm{Y}^{q+})}{M(\mathrm{X}^{p+})}, \quad (1)$$

where X and Y denote the partner fragment ions, M is the mass of the two fragment ions, and p and q are the charge number of the two fragment ions. According to eqn (1), the two fragment ions $C_2H_4{}^{81}Br^+$ ($m/q = 109$, KER = 0.71 eV) and $^{81}Br^+$ ($m/q = 81$,

KER = 1.01 eV) from C–Br bond fission can be assigned to the two-body CE process of doubly charged parent ion

$$C_2H_4Br_2 \rightarrow C_2H_4Br^+ + Br^+ + 2e^- \text{ (1.82 eV)}. \quad (2)$$

Employing the same method, the two fragment ions $C_2H_4^+$ ($m/q = 28$, KER = 1.51 eV) and $^{81}Br_2^+$ ($m/q = 162$, KER = 0.26 eV) from two C–Br bond fissions can also be verified as a two-body CE process[25]

$$C_2H_4Br_2 \rightarrow Br_2^+ + C_2H_4^+ + 2e^- \text{ (1.77 eV)}. \quad (3)$$

However, for the fragment ion $CH_2{}^{81}Br^+$ ($m/q = 109$, KER = 0.90 eV), the C–C bond fission of the doubly changed parent ion should generate two identical fragment ions $CH_2{}^{81}Br^+$, and thus it can be assigned to such a two-body CE process

$$C_2H_4Br_2 \rightarrow CH_4Br^+ + CH_2Br^+ + 2e^- \text{ (1.80 eV)}. \quad (4)$$

As can be seen, all these photodissociation channels shown above come from the CE process of the doubly charged parent ions, but their total KERs are different, which indicate that these CE channels should result from the different precursor states of the doubly charged parent ions, and this phenomenon has been observed in the previous works.[30,31] In addition, it is noted that an extra peak of the fragment ion $C_2H_4^+$ ($m/q = 28$, KER = 1.22 eV) in Fig. 2h can be observed, its forming process is relatively complex, which may come from the secondary dissociation of $C_2H_4Br^+$, the different repulsive states of the doubly charged parent ions or the complex Br_2^+ elimination process.[25]

In addition to the KER distribution, the angular distribution of the fragment ions is also important method to assign the photodissociation channel, which can show the instantaneous spatial distribution of the fragment ions at the CE moment for the two fragment ions from the same two-body CE process, their angular distributions should be consistent. Fig. 3 shows the angular distributions of the partner fragment ions $C_2H_4{}^{81}Br^+$ and $^{81}Br^+$ (a), as well as those of the partner fragment ions $C_2H_4{}^{81}Br^+$ and $^{81}Br^+$ (b). As expected, the two fragment ions that originated from the same two-body CE process exhibit a similar angular distribution, which can further confirm the above photodissociation channel assignments.

For the photodissociation process under the intense femtosecond laser field, the neutral molecules can also be ionized to the singly charged parent ions, and then dissociate into a neutral fragment and a singly charged fragment ion by the rest laser energy or the repulsive states of the singly charged parent ions. In this DI process, the KERs of the fragment ions are usually relative low. Thus, the fragment ions $C_2H_4{}^{81}Br^+$ (0 eV) and $^{81}Br^+$ (0.29 eV) from the C–Br bond fission could be assigned to the DI process of singly charged parent ion

$$C_2H_4Br_2 \rightarrow C_2H_4Br^+ + Br + e^-, \quad (5)$$

$$C_2H_4Br_2 \rightarrow C_2H_4Br + Br^+ + e^-. \quad (6)$$

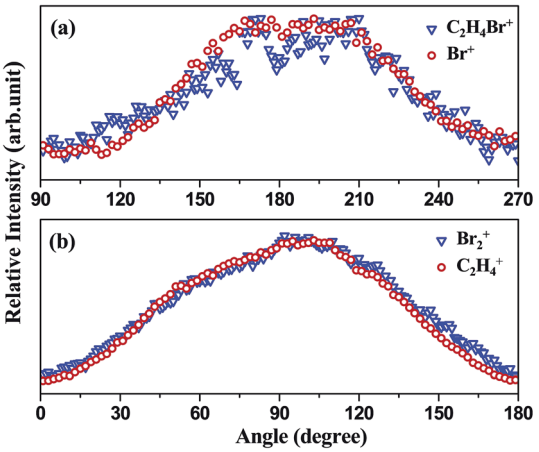

Fig. 3 The angular distributions of the fragment ions $C_2H_4Br^+$ and Br^+ with high-KER component (a) at the laser intensity of 1.3 × 10^{14} W cm^{-2}, together with the fragment ions $C_2H_4^+$ and Br_2^+ (b).

Similarly, the fragment ion $C_2H_4^+$ (0.09 eV) from the two C–Br bond fissions and the fragment ion $CH_2{}^{81}Br^+$ (0 eV) from C–C bond fission can also be respectively assigned to the DI process

$$C_2H_4Br_2 \rightarrow C_2H_4^+ + Br_2 + e^-, \quad (7)$$

$$C_2H_4Br_2 \rightarrow CH_2Br^+ + CH_2Br + e^-. \quad (8)$$

In order to further confirm above photodissociation channel assignments in the DI process, we theoretically calculate the appearance energy of these channels (5)–(8) by GAUSSIAN 09 software packages.[32] The optimized geometries of the related fragments are obtained at the level of B3LYP/6-311++G (2df, 2pd),[33–35] and the energies are further refined by CCSD(T)/cc-pVTZ with B3LYP/6-311++G (2df, 2pd) zero-point energy corrections. Here, in order to consider the scalar effect caused by the heavy Br atoms, we calculate the electronic structure of the Br atoms with relativistic pseudo-potential basis set cc-PVTZ-PP[36] obtained from the EMSL Basis Set Exchange (http://bse.pnl.gov/bse/portal). Considering the laser bandwidth and wavelength in our experiment, the available energy can be calculated from the corresponding appearance energy of the DI channels. If the electron recoil is not considered, *i.e.*, only two fragments are involved in each photodissociation channel, the KER value of the photodissociation channels can be obtained from our experimental data in Fig. 2. The appearance energy, available energy and KER value of these channels (5)–(8) are listed in Table 1. It can be seen that the KER values of these channels are all in the range of the available energies, which further indicate that the low KER components of these fragment ions should result from the DI process of 1,2-$C_2H_4Br_2$.

In all these photodissociation channels, the DI process leading to $C_2H_4^+$ and Br_2 is the most complex, which involves the two C–Br bond breaking and a new Br–Br bond forming in a kinetic step. In order to further understand how 1,2-$C_2H_4Br_2$ → $C_2H_4^+$ + Br_2 elimination channel is produced, a quantum chemical calculation at B3LYP/6-311++G (2df, 2pd) level is

Table 1 The appearance energy, the available energy and the corresponding KERs for different DI channels

Channel	Appearance energy (eV)	Available energy (eV)	KERs (eV)
(5)	10.47	0.11–0.67	0–0.12
(6)	16.12	0.49–1.35	0.21–0.91
(7)	11.54	0.54–1.17	0.04–0.21
(8)	12.19	0–0.53	0–0.03

performed by GAUSSIAN 09 software packages. Similarly, we also take into account the scalar relativistic effect caused by the heavy Br atoms by utilizing relativistic pseudo-potential basis set cc-PVTZ-PP. The geometries of the reactants, transition states and photodissociation products on the ground doublet potential energy surface (PES) of the singly charged parent ions are optimized, and the vibrational frequencies are used to characterize the stationary points, here the number of imaginary frequency NIMAG = 0 and 1 represent the local minima and the transition states, respectively. The intrinsic reaction coordinate (IRC) calculation is used to track the minimum energy path from the transition states to the corresponding minima. All single-point energies are computed by using CCSD(T) method, and the C and H atoms are calculated with cc-PVTZ basis set while the Br atoms are calculated with cc-PVTZ-PP basis sets, where these energies also include B3LYP zero-point energy corrections.

The ϕ(BrCCBr) dihedral angle, the C–Br bond lengths and the Br–Br distance are three critical parameters to characterize the structure of the 1,2-$C_2H_4Br_2$ molecule, and therefore are used to show the structure changes in the photodissociation process. Fig. 4 shows the reaction mechanism for the photodissociation process of the 1,2-$C_2H_4Br_2$ molecule to $C_2H_4^+$ and Br_2. The neutral 1,2-$C_2H_4Br_2$ molecule is first ionized to the singly charged parent ion 1,2-$C_2H_4Br_2^+$, and then becomes the *gauche*-$C_2H_4Br_2^+$ ion by a isomerization process (TS1), and finally dissociates to $C_2H_4^+$ and Br_2 by surpassing an energy barrier (TS2). The three parameter changes involving the ϕ(BrCCBr) dihedral angle, the C–Br bond lengths and the Br–Br distance in the photodissociation channel are listed in Table 2. One can see that the two Br atoms are not simultaneously produced, *i.e.*, one C–Br bond first breaks and then a new Br–Br bond is formed while the other C–Br bond still exist. Thus, the $C_2H_4Br_2 \rightarrow C_2H_4^+ + Br_2$ elimination channel is produced by an asynchronous concerted mechanism. Furthermore, in our calculation, employing MP2 level of theory at 6-311G (d, p) basis set can obtain the similar results, which can further verify our above conclusion.

Table 2 Molecular structure changes represented by the three main parameters (ϕ(BrCCBr) dihedral angle, C–Br bond lengths and Br–Br distance) along the reaction coordinates using B3LYP method. The C and H atoms are calculated by 6-311++G (2df, 2pd) basis set while the Br atoms are calculated by relativistic pseudo-potential cc-PVTZ-PP basis set

Molecular structures	ϕ(BrCCBr) dihedral angle (°)	C–Br bond lengths (Å)	Br–Br distance (Å)
Anti-1,2-$C_2H_4Br_2$	180	1.98, 1.98	4.67
Anti-1,2-$C_2H_4Br_2^+$	167	1.96, 1.96	4.58
TS1	124	1.93, 1.96	4.31
gauche-1,2-$C_2H_4Br_2^+$	40	2.00, 2.00	2.89
TS2	12	2.11, 2.74	2.50

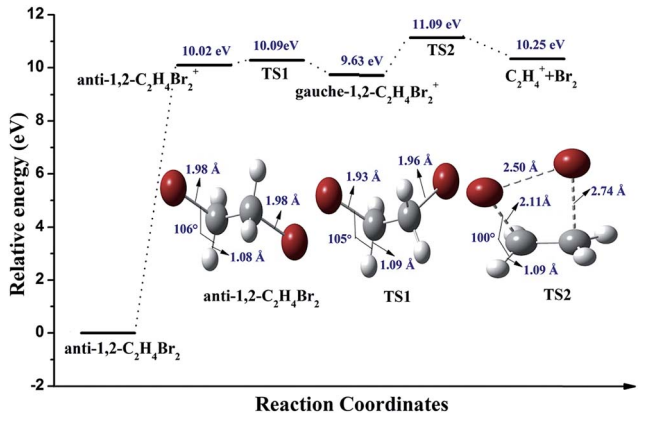

Fig. 4 Reaction mechanism for the dissociation pathway of 1,2-$C_2H_4Br_2$ to $C_2H_4^+$ and Br_2 including the relevant energies. The geometries are optimized with B3LYP functional, and the C and H atoms are calculated with 6-311++G (2df, 2pd) basis set while the Br atoms are calculated with cc-PVTZ-PP basis set. All single-point energies are computed by using CCSD(T) method, and the C and H atoms are calculated with cc-PVTZ basis set while the Br atoms are calculated with cc-PVTZ-PP basis sets, where the energies include B3LYP zero-point energy corrections.

IV. Conclusion

In summary, the molecular photodissociation of 1,2-$C_2H_4Br_2$ have been experimentally investigated in near-infrared (800 nm) femtosecond laser field by the dc-slice imaging technology. These fragment ions $C_2H_4Br^+$, Br^+, $C_2H_4^+$, Br_2^+ and CH_2Br^+ were measured and their corresponding KERs and angular distributions were calculated. By observing the KERs and angular distributions, it was confirmed that these fragment ions with high KERs result from the CE process of the doubly charged parent ion 1,2-$C_2H_4Br_2^{2+}$ while those with low KERs result from the DI process of the singly charged parent ion 1,2-$C_2H_4Br_2^+$. Furthermore, *ab initio* calculations were carried out to simulate the DI process leading to $C_2H_4^+$ and Br_2 on the ground doublet PES of 1,2-$C_2H_4Br_2^+$, it was shown that the neutral 1,2-$C_2H_4Br_2$ molecule is first ionized to the singly charged parent ion 1,2-$C_2H_4Br_2^+$, and then 1,2-$C_2H_4Br_2^+$ overcomes an energy barrier to dissociate *via* an asynchronous concerted mechanism after undergoing isomerization. We believe that these experimental and theoretical results are useful to understand the photodissociation process of the hydrocarbon bromide molecule and are expected to be significant for understanding and controlling the photochemical reaction.

Acknowledgements

This work was partly supported by National Natural Science Fund (no. 11004060 and 11027403), Shanghai Municipal Science and Technology Commission (no. 14JC1401500), and Shanghai Rising-Star Program (no. 12QA1400900).

References

1 M. Castillejo, S. Couris, E. Koudoumas and M. Martin, *Chem. Phys. Lett.*, 1998, **289**, 303.
2 K. Vijayalakshmi, C. P. Safvan, K. G. Ravindra and D. Mathur, *Chem. Phys. Lett.*, 1997, **270**, 37.
3 T. Zuo and A. D. Bandrauk, *Phys. Rev. A*, 1995, **52**, R2511.
4 W. G. Roeterdink and M. H. M. Janssen, *Phys. Chem. Chem. Phys.*, 2002, **4**, 601.
5 P. Tzallas, C. Kosmidis, J. G. Philis, K. W. D. Ledingham, T. McCanny, R. P. Singhal, S. M. Hankin, P. F. Taday and A. J. Langley, *Chem. Phys. Lett.*, 2001, **343**, 91.
6 C. Wu, C. Y. Wu, D. Song, H. M. Su, Y. D. Yang, Z. F. Wu, X. R. Liu, H. Liu, M. Li, Y. K. Deng, Y. Q. Liu, Y. P. Liang, H. B. Jiang and Q. H. Gong, *Phys. Rev. Lett.*, 2013, **110**, 103601.
7 S. C. Wofsy, M. B. McElroy and Y. L. Yung, *Geophys. Res. Lett.*, 1975, **2**, 215.
8 Y. L. Yung, J. P. Pinto, R. J. Watson and S. P. Sander, *J. Atmos. Sci.*, 1980, **37**, 339.
9 J. C. van der Leun, *Photodermatol., Photoimmunol. Photomed.*, 2004, **20**, 159.
10 T. Gougousi, P. C. Samartzis and T. N. Kitsopoulos, *J. Chem. Phys.*, 1998, **108**, 5742.
11 J. G. Underwood and I. Powis, *Phys. Chem. Chem. Phys.*, 2000, **2**, 747.
12 W. P. Hess, D. W. Chandler and J. W. Thoman, *Chem. Phys.*, 1985, **163**, 277.
13 P. Y. Wei, Y. P. Chang, W. B. Lee, Z. F. Hu, H. Y. Huang, K. C. Lin, K. T. Chen and A. H. H. Chang, *J. Chem. Phys.*, 2006, **125**, 133319.
14 C. Y. Hsu, H. Y. Huang and K. C. Lin, *J. Chem. Phys.*, 2005, **123**, 134312.
15 H. Y. Huang, W. T. Chuang, R. C. Sharma, C. Y. Hsu, K. C. Lin and C. H. Hu, *J. Chem. Phys.*, 2004, **121**, 5253.
16 D. Xu, J. S. Francisco, J. Huang and W. M. Jackson, *J. Chem. Phys.*, 2002, **117**, 2578.
17 Y. M. Wang, S. Zhang, Q. S. Zheng and B. Zhang, *Chem. Phys. Lett.*, 2006, **423**, 106.
18 Y. R. Lee, C. C. Chen and S. M. Lin, *J. Chem. Phys.*, 2003, **118**, 10494.
19 Y. R. Lee, C. C. Chen and S. M. Lin, *J. Chem. Phys.*, 2004, **120**, 1223.
20 H. L. Lee, P. C. Lee, P. Y. Tsai, K. C. Lin, H. H. Kuo, P. H. Chen and A. H. H. Chang, *J. Chem. Phys.*, 2009, **130**, 184308.
21 A. T. J. B. Eppink and D. H. Parker, *Rev. Sci. Instrum.*, 1997, **68**, 3477.
22 D. H. Parker and A. T. J. B. Eppink, *J. Chem. Phys.*, 1997, **107**, 2357.
23 Y. Yang, L. L. Fan, S. Z. Sun, J. Zhang, Y. T. Chen, S. A. Zhang, T. Q. Jia and Z. R. Sun, *J. Chem. Phys.*, 2011, **135**, 064303.
24 S. Z. Sun, Y. Yang, J. Zhang, H. Wu, Y. T. Chen, S. A. Zhang, T. Q. Jia, Z. G. Wang and Z. R. Sun, *Chem. Phys. Lett.*, 2013, **581**, 16.
25 H. Wu, Y. Yang, S. Z. Sun, J. Zhang, L. Deng, S. A. Zhang, T. Q. Jia, Z. G. Wang and Z. R. Sun, *Chem. Phys. Lett.*, 2014, **607**, 70.
26 C. L. Guo, M. Li, J. P. Nibarger and G. N. Gibson, *Phys. Rev. A*, 1998, **58**, R4271.
27 Y. M. Wang, S. Zhang, Z. R. Wei and B. Zhang, *J. Phys. Chem. A*, 2008, **112**, 3846.
28 Y. M. Wang, S. Zhang, Z. R. Wei and B. Zhang, *Chem. Phys. Lett.*, 2009, **468**, 14.
29 M. E. Corrales, G. Gitzinger, J. G. Vazquez, V. Loriot, R. de Nalda and L. Banares, *J. Phys. Chem. A*, 2012, **116**, 2669.
30 Y. Furukawa, K. Hoshina, K. Yamanouchi and H. Nakano, *Chem. Phys. Lett.*, 2005, **414**, 117.
31 T. Okino, *et al.*, *Chem. Phys. Lett.*, 2006, **419**, 223.
32 M. J. Frisch, G. W. Trucks, H. B. Schlegel, G. E. Scuseria, M. A. Robb, J. R. Cheeseman, G. Scalmani, V. Barone, B. Mennucci, G. A. Petersson, H. Nakatsuji and M. Caricato, *et al.*, *Gaussian 09, Revision B.01*, Gaussian, Inc., Wallingford CT, 2010.
33 A. D. Becke, *J. Chem. Phys.*, 1993, **98**, 5648.
34 C. Lee, W. Yang and R. G. Parr, *Phys. Rev. B: Condens. Matter Mater. Phys.*, 1988, **37**, 785.
35 L. Q. Hua, W. B. Lee, M. H. Chao, B. Zhang and K. C. Lin, *J. Chem. Phys.*, 2011, **134**, 194312.
36 K. A. Peterson, D. Figgen, E. Goll, H. Stoll and M. Dolg, *J. Chem. Phys.*, 2003, **119**, 11113.